Eur. Phys. J. Special Topics **225**, 1693–1705 (2016)

DOI: 10.1140/epjst/e2016-60150-1

THE EUROPEAN PHYSICAL JOURNAL SPECIAL TOPICS

Regular Article

Static polarizability effects on counterion distributions near charged dielectric surfaces: A coarse-grained Molecular Dynamics study employing the Drude model

José Rafael Bordin[1,a], Rudolf Podgornik[2,b], and Christian Holm[3,c]

[1] Campus Caçapava do Sul, Universidade Federal do Pampa, Rua Pedro Anunciação 111, CEP 96570-000, Caçapava do Sul, Brazil
[2] Department of Physics, Faculty for Mathematics and Physics, University of Ljubljana, Jadranska 19, 1000 Ljubljana and Department of Theoretical Physics, J. Stefan Institute, 1000 Ljubljana, Slovenia
[3] Institut für Computerphysik, Universität Stuttgart, Allmandring 3, 70569 Stuttgart, Germany

Received 30 April 2016 / Received in final form 4 July 2016
Published online 10 October 2016

Abstract. Coarse-grained implicit solvent Molecular Dynamics (MD) simulations have been used to investigate the structure of the vicinal layer of polarizable counterions close to a charged interface. The classical Drude oscillator model was implemented to describe the static excess polarizability of the ions. The electrostatic layer correction with image charges (ELCIC) method was used to include the effects of the dielectric discontinuity between the aqueous solution and the bounding interfaces for the calculation of the electrostatic interactions. Cases with one or two charged bounding interfaces were investigated. The counterion density profile in the vicinity of the interfaces with different surface charge values was found to depend on the ionic polarizability. Ionic polarization effects are found to be relevant for ions with high excess polarizability near surfaces with high surface charge.

1 Introduction

A detailed understanding of the electric double layer (EDL) is necessary for the study of a variety of systems, including colloidal suspensions, as well as charged biological macromolecules and membranes [1,2]. While the mean-field Poisson-Boltzmann (PB) formalism [3,4] is traditionally invoked to analyze the electrostatic interactions in such systems, it is also subject to severe shortcomings due to its neglect of electrostatic correlations and ionic size, hence it can be unreliable in its fundamental

[a] e-mail: josebordin@unipampa.edu.br
[b] e-mail: rudolf.podgornik@ijs.si
[c] e-mail: holm@icp.uni-stuttgart.de

predictions. Despite these shortcomings, the PB theory properly describes the behavior of Coulomb fluids composed of monovalent ions at low concentrations in the vicinity of weakly charged interfaces, while for strongly charged systems, where correlation and finite size effects begin to dominate the overall behavior of the system, the PB theory is simply inappropriate [3,5–8]. While attempts at improving the PB theory have been formulated to amend its shortcomings in various contexts [8–20], coarse grained implicit solvent simulations still provide the baseline for assessing the validity of all approximate analytical theories.

Charged particles immersed in an aqueous solution possess a local (static) polarizability that can be significantly lower than that of water. In fact, since Debye's seminal analysis (see the discussion in Ref. [21]), the ion polarizability effects have been known to play an important role in the description of ionic solutions. In particular, for the description of ion-specific effects they are completely ignored by the PB analytical approach [8], but are just as difficult to properly implement in atomistic and/or coarse-grained simulations. Furthermore, ionic polarizability and the size of the ions are parameters that distinguish between ions of the same valency and thus describe some of the ion-specific features of electrostatic interactions. On the analytical side, there have been recent advances to include ion polarizabilities on the mean-field PB level based on the ionic decrement of the dielectric constant [21–23], which, however, can not include the effect of dielectric inhomogeneities that have to be implemented in a more general setting [24–27], that goes beyond the mean-field approximation and is formally much more demanding, giving explicit results only in the asymptotic limits of weak and strong coupling [28]. The difficulties on the computer simulation side have other reasons that could be mostly seen as twofold: first of all, the consistent inclusion of dielectric inhomogeneities presupposes a detailed calculation of the image effects that involve the full solution of the Poisson equation on the fly, and second, the consistent inclusion of the ion polarizabilities represents a non-pairwise additive effect that needs to be properly implemented into the simulation code in order to retain the essential features of its many-body nature. While these outstanding problems are not easy to surmount, even for coarse-grained Monte Carlo (MC) and/or Molecular Dynamics (MD) computer simulations, requiring a significant computational effort, there have been important recent advances in the simulation methodology that can appropriately deal with image charges, dielectric discontinuities and local polarizabilities [11,27,29–39]. While numerous simulations have shown how the ionic size can influence the ion density profile near a charged interface [9,16,40–42], the ion polarization effects have been more difficult to handle and the progress slower; see Refs. [24,25,31] for recent advances, describing different cases of ion polarizability effects. Also for atomistic simulations, of course, polarization effects turn out to be crucial under certain circumstances, e.g. ions at an air-water interface or in ion channes, to name a few [43–47].

Our goal in this work is to use a simple coarse-grained model for MD simulations of polarizable charged particles and apply it to the study of the counterion density profile near charged interfaces. The low computational cost of coarse-grained models allows us to simulate large systems over long simulation times at low computational costs, which makes them particularly appropriate for the simulation of systems with long-range and non-pairwise additive interactions. The particular implementation of the static ionic polarizability that we consider in detail is the classical *Drude oscillator model* [48]. It was proposed initially for polarizable water models in classical all-atom MD simulations [43–46], but was later used more generally to include ionic polarizability affects and hydration properties of bulk electrolytes solutions [49,50], to describe the interaction of ions with the water surface [51], and with biological molecules [52,53], as well as to study the properties of polarizable ionic liquids [54,55]. A detailed review of theories and applications of several polarizable models to

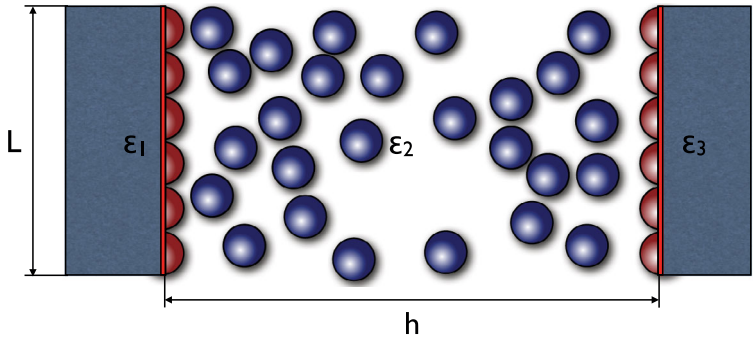

Fig. 1. Schematic depiction of the simulation box with counterions confined in a planar slab geometry of width h. The counterions are immersed in a dielectric medium with dielectric constant $\epsilon_2 = 80$ (water) while the external layers have a different dielectric constant, viz. $\epsilon_1 = 2$ in the left and $\epsilon_3 = 2$ or $\epsilon_3 = 80$ in the right semi-infinite layers. The fixed charge on both interfaces is described with finite-size charged spheres of charge $q_w e$, where e is the elementary charge, and diameter $a_w = 0.425\,\text{nm}$, located at the dielectric interface.

coarse-grained MD simulations can be found in Ref. [56] and for classical Drude oscillators in Ref. [47]. In this paper we specifically present an implementation of the Drude oscillator model in the coarse-grained simulation package ESPResSo [57–59] and use it to investigate the polarizability effects in the counterion distribution near charged interfaces together with the electrostatic layer correction with image charges (ELCIC) [35] to treat the image charge effect in the presence of 2D dielectric bounding interfaces. We restrict ourselves to canonical counterion-only systems confined either by one or two charged (dielectric) interfaces.

The paper is organized as follow. The polarizable model and simulational details are presented in Sect. 2, including the details of the implementation of the Drude oscillators. Our results are then discussed in Sect. 3, and we summarize our work in the final Sect. 4.

2 Model and simulation details

2.1 Model system

We use a Drude oscillator model to describe polarizable ions confined to a slab geometry. The counterions are placed in an implicit solvent finite width homogeneous dielectric slab with dielectric constant ϵ_2, surrounded by external semi-infinite dielectric media with dielectric constants ϵ_1 and ϵ_3. The simulation cell is a cuboid with dimensions $L \times L \times h$ in the x, y, and z-directions, respectively. Confining walls are placed at the boundaries of the box in the z-direction and are constructed as planar sheets of explicit ions with charge $q_w e$, where $e = 1.6 \times 10^{-19}\,\text{C}$, and diameter a_w. This model is a good approximation for ions near charged macroions or inside charged nanopores. A schematic 2-d projection of the simulation box is shown in Fig. 1.

Different cases of the canonical simulation box were studied. In the first case, only one confining wall is charged, with a surface charge density $\sigma_s = q_w e/(\pi a_w^2)$, and the other one is electrically neutral, with a separation h between the walls of value $h = 12.75\,\text{nm}$, to simulate counterions near a macromolecular surface. The second case has both walls charged, with $h = 4.25\,\text{nm}$, to simulate counterions in confinement, inside a charged nanopore or surrounded by two large macroions. In both cases, the walls are constructed using N_w fixed particles with diameter $a_w = 0.425\,\text{nm}$, with the

extent in the x and y direction being $L = 8.5\,\mathrm{nm}$. Standard periodic boundary conditions were applied in the x and y directions. N polarizable counterions with diameter $a = 0.425\,\mathrm{nm}$ and charge qe, with $q = 1$ or 2, are placed in the homogeneous dielectric continuum solvent confined by the walls, so that the system is overall electrically neutral.

2.2 Interaction potentials

The electrostatic interaction energy between the counterion i and the counterion/wall particle j is described by the standard Coulomb potential

$$U_{ij}^{\mathrm{C}}(r) = l_B k_B T \frac{q_i q_j}{r} \tag{1}$$

where $l_B = e^2/4\pi\epsilon_0\epsilon k_B T = 7.14\,\text{Å}$ is the Bjerrum length at temperature $T = 298\,\mathrm{K}$ and k_B is the Boltzmann constant. The short-range repulsion was modeled using the Weeks-Chandler-Andersen potential $U_{ij}^{\mathrm{WCA}}(r)$ [61]

$$U_{ij}^{\mathrm{WCA}}(r) = \begin{cases} U_{\mathrm{LJ}}(r) - U_{\mathrm{LJ}}(r_c) & \forall\, r \le r_c, \\ 0 & \forall\, r > r_c, \end{cases} \tag{2}$$

where $U_{\mathrm{LJ}}(r)$ is the standard 12-6 LJ potential, $r_c = 2^{1/6} a_{ij}$, $a_{ij} = 0.5(a_i + a_j)$ and $\epsilon = 1 k_b T$. The Coulomb potential, (1), was evaluated using the three-dimensional P3M method [60], and the correction terms for a slab-like system with image charges due to the presence of a dielectric discontinuity were taken into account by using the ELCIC method [35].

One of the major advantages of the Drude model is its simplicity. The inclusion of the polarizability of the atoms is done via one mobile ion pair (Drude dipole) per (coarse-grained) atom whose electrostatic interactions can be treated using standard electrostatic algorithms.

2.3 Drude model and its ESPResSo implementation

The static polarizability of the counterions was modeled via the classical Drude oscillator model [43–46,48–51,54,55,62]. In this model, the static polarization α of an ion with charge q is described by a Drude particle, with charge q_D and mass m_D, attached to the ion core. To conserve the net charge of the ion-Drude particle pair, the charge of the ion core is replaced by $q - q_D$, see Fig. 2. The Drude particle is connected to the ion by a harmonic potential

$$U^{\mathrm{bond}}(\mathbf{r}, \mathbf{d}) = \tfrac{1}{2} k_D \left|\mathbf{r} - \mathbf{d}\right|^2 \tag{3}$$

with a large force constant k_D, constraining the value of the charge q_D of the Drude particle to reproduce the correct value of α via [43]

$$\alpha = \frac{q_D^2}{k_D}. \tag{4}$$

In the absence of an electric field, the Drude particle oscillates around the position of the core, and the pair appears as a point-like ion with charge q. When an external electric field $\mathbf{E}$ is applied, the Drude particle oscillates around the position $\mathbf{d} = q_D \mathbf{E}/k_d$, with a dipole moment $\mu = q_D^2 \mathbf{E}/k_d$. $\mathbf{E}$ is the total electric field at the position of the

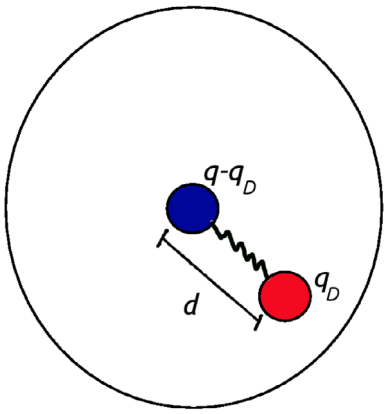

Fig. 2. Example of a polarizable ion described by the classical Drude model, with an exaggerated displacement d of the Drude particle q_D attached to the center of the ion.

Drude particle. The value of k_D is chosen such that the distance between the core and the Drude particle $\mathbf{d_i}$ is much smaller than the size of the ion. As a result, the induced dipole of dipolar moment μ behaves as a point-like dipolar particle.

While the energy of the classical Drude model of a polarizable particle, (3), looks deceptively simple, it actually corresponds to non-pairwise additive interactions between polarizable particles. In fact, the electric field $\mathbf{E}$ in a certain configuration of a many-particle system has contributions from all the particles in the system, including all other Drude particles. The non-pairwise nature of this interaction emerges since at each step of the simulation, the local electric field at the position of the Drude particle i induces a dipolar moment that then interacts with all the other Drude particles, $j \neq i$, which then in turn change the dipolar moment of the original Drude particle i and so on.

Our implementation of the Drude model follows previous works and was adapted to the ESPResSo package. The self-consistent field (SCF) regime is required to study induced static polarizability, but is computationally expensive and strongly affects the energy conservation and the stability of the temperature imposed by the thermostat [43]. To avoid this problem, we used a stochastic Langevin thermostat as proposed by Jiang et al. [62] to achieve a SCF-like dynamics. A dual Langevin thermostat procedure was used to keep the ions of the system at a high temperature, $T = 300\,\mathrm{K}$, and a colder thermostat at temperature $T^* = 1\,\mathrm{K}$ was applied to the Drude oscillators. The preservation of the lower value T^* depends mainly on the balance between energy gained due to electrostatic interactions with other particles and energy losses due to the damping term in the Langevin thermostat. We should note that recently an alternative to the Langevin Dynamics, namely an implementation using an extended Lagrangian Dynamics, was proposed [63].

The Molecular Dynamics simulations were performed using a time step $\delta t = 1.0\,\mathrm{fs}$. At time $t = 0$ the counterions were distributed randomly between the walls, and an initial 0.1 ns MD run was performed to equilibrate the system. The density profiles are then obtained by a 10 ns MD production run. Each resulting density profile was obtained by averaging five independent simulations and taking the mean.

2.4 Simulation details

The dynamics of the system was implemented as follows. The coordinates of each ion-Drude pair, $\mathbf{r}_i$ and $\mathbf{r}_{i,\mathbf{D}}$, were separated in terms of the center of mass position, $\mathbf{R}_i$,

and the relative distance between the pair of charges, $\mathbf{d}_i = \mathbf{r}_{i,D} - \mathbf{r}_i$. The corresponding equations of motion can be expressed as

$$M_i \ddot{\mathbf{R}}_i = \mathbf{F}_{\mathbf{R},i} - \gamma \dot{\mathbf{R}}_i + \mathbf{f}_i, \tag{5}$$

$$m_i \ddot{\mathbf{d}}_i = \mathbf{F}_{\mathbf{d},i} - \gamma' \dot{\mathbf{d}}_i + \mathbf{f}'_i. \tag{6}$$

In these expressions, M_i is the total mass of the pair, $m_i = m_D(1 - m_D/M_i)$ the reduced mass of the oscillator, $\mathbf{F}_{\mathbf{R},i}$ and $\mathbf{F}_{\mathbf{d},i}$ the resulting force on the center of mass and on the reduced mass, γ is the external Langevin friction coefficient and γ' the internal Langevin friction coefficient. The white noise responsible for the damping terms in the thermostats is represented by fluctuating random forces, $\mathbf{f}_i = (2\gamma k_B T/M_i)^{1/2} G(t)$ and $\mathbf{f}'_i = (2\gamma' k_B T^*/m_i)^{1/2} G^*(t)$. $G(t)$ and $G^*(t)$ are univariate Gaussian random processes. Using the chain rule, we can express the forces in the center of mass coordinates and displacements in terms of the actual forces on the particles

$$\mathbf{F}_{\mathbf{R},i} = -\left(\frac{\partial U}{\partial \mathbf{r}_i}\right) - \left(\frac{\partial U}{\partial \mathbf{r}_{i,\mathbf{D}}}\right),$$

$$\mathbf{F}_{\mathbf{d},i} = -\left(1 - \frac{m_D}{M_i}\right)\left(\frac{\partial U}{\partial \mathbf{r}_{i,\mathbf{D}}}\right) + \left(\frac{m_D}{M_i}\right)\left(\frac{\partial U}{\partial \mathbf{r}_i}\right), \tag{7}$$

where the total potential energy of the system then has the form

$$U = \sum_{i \neq j} U_{ij}^{\mathrm{C}}(\mathbf{r}_{ij}) + \sum_{i \neq j} U_{ij}^{\mathrm{WCA}}(\mathbf{r}_{ij}) + \sum_i U_i^{\mathrm{bond}}(\mathbf{r}_i, \mathbf{d}(\mathbf{E}_i)). \tag{8}$$

Here, $\mathbf{E}$ is the total electrostatic field at the position of the particle, i.e.

$$\mathbf{E}_i = -\boldsymbol{\nabla} \sum_j l_B k_B T \frac{q_j}{r_{ij}}. \tag{9}$$

The first term in Eq. (8) corresponds to the electrostatic interactions between all charges in the system, U^{WCA} is the excluded volume term and U^{bond} is the ion-Drude particle harmonic potential. The equations of motion, Eqs. (5) and (6), can then be rewritten in terms of the real coordinates of the particles in the form [43]

$$\mathbf{r}_i = \mathbf{R}_i - \left(\frac{m_D}{M_i}\right)\mathbf{d}_i,$$

$$\mathbf{r}_{i,\mathbf{D}} = \mathbf{R}_i + \left(1 + \frac{m_D}{M_i}\right)\mathbf{d}_i. \tag{10}$$

The integration of the center of mass and displacements for the Drude oscillators is identical to the integration of standard particles [62], and is thus already implemented in the ESPResSo package, also for the case of a dual Langevin thermostat [57]. The integration of the equations of motion for the Drude oscillators is also straightforward. In all simulations we set $k_D = 10^5$ kcal/mol/Å^2 for the ions.

3 Results and discussion

The first system under study consists of monovalent counterions in a system with only one charged wall. Typical values of surface charge density for colloidal systems [64,65]

were used, $\sigma_s = 0.1$, 0.2, 0.3 or $0.4\,\mathrm{C/m^2}$. The counterions, with polarizability α and charge $-e$, are placed in the implicit solvent with dielectric constant $\epsilon_2 = 80$. No extra salt was added to the system. The values of the polarizability of ions in aqueous solution were recently obtained by quantum chemical calculation [66]. For the halide anions the ionic polarizabilities α_{ci} amount to: fluoride $\alpha_{ci} = 1.3\,\text{Å}^3$, chlorine $\alpha_{ci} = 3.5\,\text{Å}^3$, bromide $\alpha_{ci} = 4.6\,\text{Å}^3$ and iodide $\alpha_{ci} = 7.5\,\text{Å}^3$, while previous work suggests slightly higher values [50]. To investigate how the ionic polarizability affects the counterion distribution in our coarse-grained model, we decided to display it using the *excess polarizability* of counterions, which is equal to the difference between the water polarizability and the ion polarizability. The values of excess polarizabilities are typically negative, since most salt ions are less polarizable then water, whose polarizability is $\alpha_w = 1.44\,\text{Å}^3$ [43]. This is also reflected in the dielectric decrement of salt solutions [21,22]. We therefore use excess ion polarizabilities in the range of $\alpha_{exc} = \alpha_w - \alpha_{ci} = 0$, -1.0, -3.5, -6.0 or $-8.5\,\text{Å}^3$ in our simulations to study systematically the influence of the excess ion polarizability with experimentally relevant values. The diameter was taken to be the same for all counterions in the simulations in order to ensure that only polarizability effects will be singled out in the comparison. In addition, for the case of a single bounding wall, we assume the dielectric constant of the semi-infinite regions as, $\epsilon_2 = \epsilon_3 = 80$, with an additional dielectric discontinuity at the bounding layer of value $\epsilon_1 = 2$.

As a test case, we studied the counterions distribution near a planar charged wall with $\sigma_s = 0.1\,\mathrm{C/m^2}$. We explore the limit of small excess ion polarizability, $\alpha_{exc} = -10^{-6}\,\text{Å}^3$, and compare with results obtained using MD simulations of non-polarizable ions. As expected, in the limit of small polarizability and small surface charge density, the results of both simulations are indistinguishable. Since the behavior of non-polarizable ions and Drude oscillators with small α_{exc} are the same, we will refer from now on to the case $\alpha_{exc} = -10^{-6}\,\text{Å}^3$ as being equivalent to $\alpha_{exc} = 0\,\text{Å}^3$.

The density profiles of the polarizable counterions for all the values of surface charge density are shown in Fig. 3. For better visualization, the curves were renormalized by the contact density for $\alpha_{exc} = 0.0\,\text{Å}^3$, namely ρ_0, in each case. Due to the dielectric discontinuity between the wall and the solvent, image charge effects need to be taken into account, and are obviously stronger for lower values of the surface charge, $\sigma_s = 0.1$ or $0.2\,\mathrm{C/m^2}$, as we can see in Fig. 3(A) and (B). The effect of the dielectric discontinuity at the interface is the image charge repulsion that tends to deplete the region in close proximity to the charged wall, leading to a sudden drop of the density in the vicinal layer next to the dielectric interface. The image charge repulsion is counteracted by the surface charge – counterion attraction and the image charge depletion effect thus tends to diminish with increasing surface charge.

Apart from the image charge effects, the ionic polarizability does not seem to play a significant role, and the density profiles of the ions are not significantly different for all values of the excess polarizability α_{exc}. When the surface charge is increased to $\sigma_s = 0.3\,\mathrm{C/m^2}$ the effect of the image charge repulsion diminishes, and the counterions can reside closer to the bounding wall due to stronger electrostatic attraction. Still, one can observe a small but consistent decrease in the contact density for counterions with higher negative excess polarizability. To see this more clearly, we explicitly show the contact density in Fig. 4 as a function of the counterion polarizability. For lower values of the surface charge, the contact density shows very little variation with ion polarizability, but when the charge density is increased, from $\sigma_s = 0.3\,\mathrm{C/m^2}$ to $\sigma_s = 0.4\,\mathrm{C/m^2}$, more pronounced and clearly discernible dependence on the excess polarizability appears. For a highly charged bounding wall, at higher absolute values of the polarizability, the contact density is reduced and the counterion cloud near the wall becomes broader, as can clearly been inferred from Fig. 3(D).

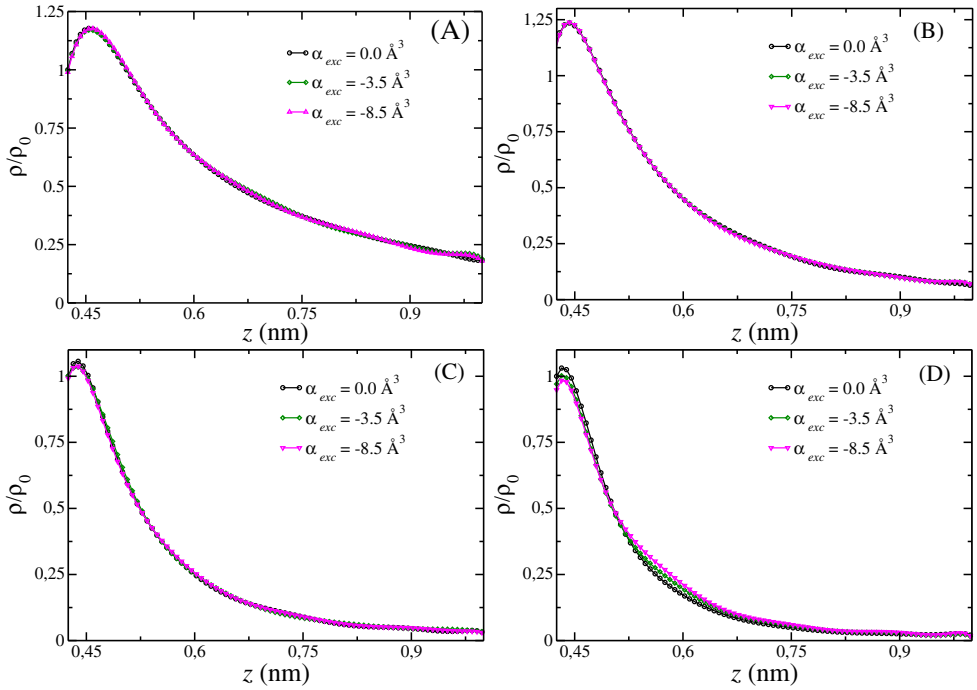

Fig. 3. Polarizable counterion density profiles near a single charged wall with $\sigma_s = 0.1$(A), 0.2(B), 0.3(C) and 0.4(D) C/m^2 as a function of the distance from the wall between 0 and 1 nm. For better visualization only the curves for $\alpha_{exc} = 0.0$, -3.5 and -8.5 Å^3 are shown.

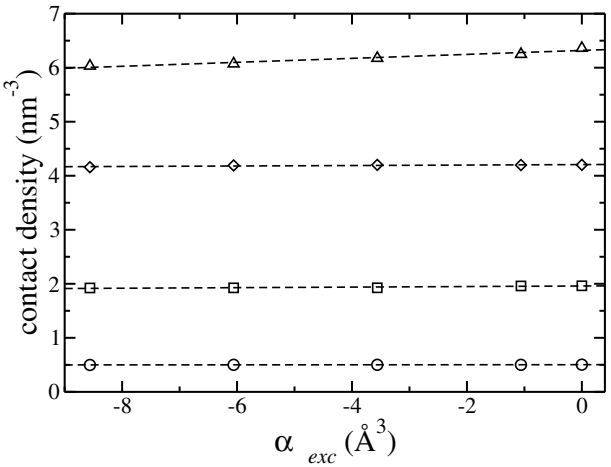

Fig. 4. Polarizable counterion contact density for different values of the surface charge density. The circles correspond to $\sigma_s = 0.1$ C/m^2, squares to $\sigma_s = 0.2$ C/m^2, diamonds to $\sigma_s = 0.3$ C/m^2 and triangles to $\sigma_s = 0.4$ C/m^2. A linear fit is also shown for each curve to help to guide the eye.

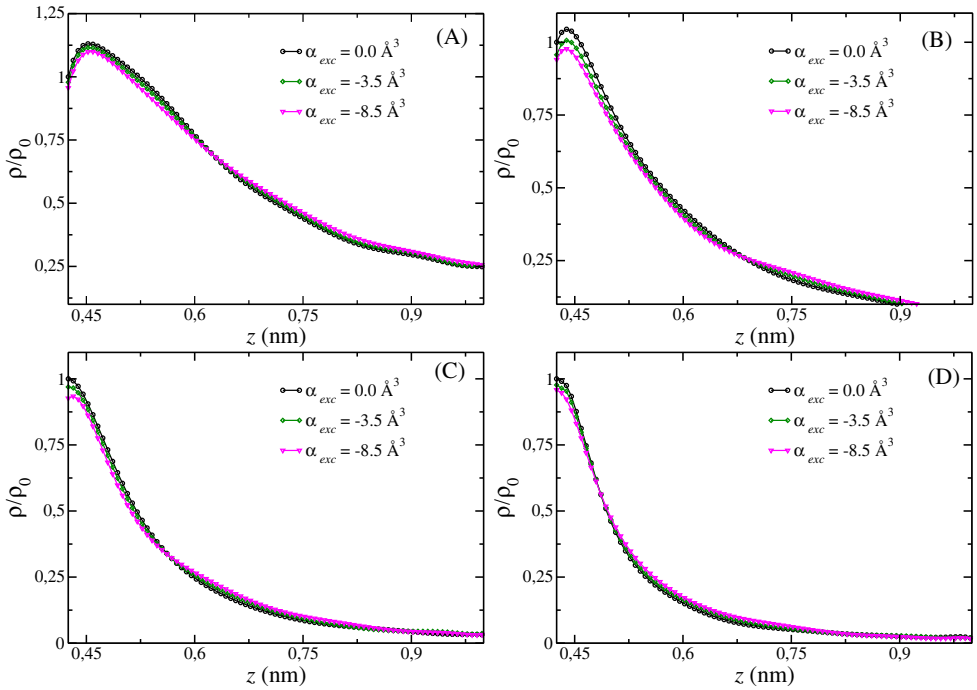

Fig. 5. Density profiles of polarizable counterions near one of the two equally charged surfaces for $\sigma_s = 0.1$(A), 0.2(B), 0.3(C) and 0.4(D) C/m^2. For better visualization only the curves for $\alpha_{exc} = 0$, -3.56 and -8.56 Å^3 are shown as well as only one side of a system with symmetric charge density distribution.

This wider density distribution of polarizable counterions near the charged wall has several reasons. The positively charged wall attracts the counterion core, with a negative charge, but also repels the Drude dipole modeling the polarizability. Monopole-monopole, monopole-dipole and dipole-dipole interactions between a counterion, the charged wall and the dielectric images of the counterion then lead to an increased attraction to the wall, and would by itself increase the contact density. However, the collective interactions between the counterion cloud and the charged dielectric interface are more complicated since the higher density of counterions, with lower polarizability than the intervening solvent, modifies also the effective solution dielectric constant by the dielectric decrement effect [21,22,28]. These combined effects then lead to an overall diminished attraction between counterions and the surface, and a broader mobile charge distribution in the vicinity of the wall results as a consequence.

In the case of two equally charged walls at small separation distance h, with confined counterions in between and with dielectric mismatch at both bounding surfaces with $\epsilon_2 = 80$, $\epsilon_1 = \epsilon_3 = 2$, the resulting counterion density distribution indicates that the polarization effects are stronger than in the case of a single charged interface. Unlike the latter case with a single charge surface of $\sigma_s = 0.2$ C/m^2, the density profile near the wall, see Fig. 5(B), shows a diffuse behavior on increase of the polarizability. Even for walls with $\sigma_s = 0.1$ C/m^2 this effect can be clearly distinguished, see Fig. 5(A). In the case of smaller charge density, $\sigma_s = 0.1$ C/m^2, the increase of the contact density with the excess polarizability, Fig. 6, shows less pronounced variation compared to the case of $\sigma_s = 0.2$ C/m^2. For two charged interfaces at small

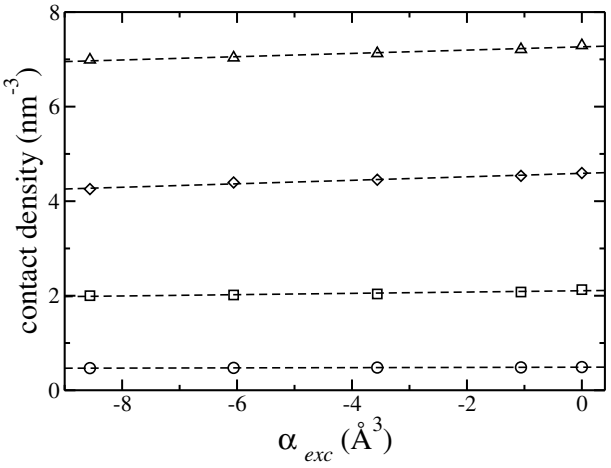

Fig. 6. Polarizable counterion contact density at the left charged interface for different values of the surface charge density. The circles correspond to $\sigma_s = 0.1\,\mathrm{C/m^2}$, squares to $\sigma_s = 0.2\,\mathrm{C/m^2}$, diamonds to $\sigma_s = 0.3\,\mathrm{C/m^2}$ and triangles to $\sigma_s = 0.3\,\mathrm{C/m^2}$. A linear fit is shown for each result to help to guide the eye.

separations h the contact density exhibits a stronger variation with the excess polarizability. This enhancement effect will, of course, vanish for larger separations of the order of a few Guy-Chapman lengths.

These results indicate that the confinement of polarizable ions in nanostructures and the dielectric discontinuity at the boundaries lead to a stronger role of counterion polarizability, stemming from the coupling between the ion polarizability and the dielectric images. The polarizability of the bounding surfaces, i.e. their dielectric constant, is thus strongly influencing the effects in the ion polarizability, so that the coupling between the two can not be neglected.

4 Conclusion

The classical Drude oscillator model for polarizability was implemented in the ESPResSo package and the results of its first application to a physical system were analyzed. We have used coarse-grained MD simulation method to study the effect of the ionic polarizability in a solution of ions confined to a slab with either one, or both of the boundaries charged. The coupling between the counterion polarizability and the dielectric polarizability of the bounding surfaces was considered within the ELCIC method. The polarizability of the mobile ions was found to play a small role in the charge density profile near charged interfaces whose significance depends on the wall and ion properties. For a proper description of ionic solutions confined inside charged nanopores or close to highly charged macroions, the effects of the ion polarizability therefore should be included, if the couplings are high enough.

The general conclusion of our work is that for surfaces with low charge density, where the interaction with the dielectric images dominates, the static polarizability of the counterion plays a minor role and can be neglected. However, for highly charged surfaces, counterions with a large polarizability exhibit a more diffuse density profile near the wall, and the ionic polarizability can in general not be neglected. This conclusion tallies nicely also with the previous approximate analytical theories based either on the mean-field PB approach [21–23], as well as those that formulate the

effects of ionic polarizability in terms of the general weak-strong coupling dichotomy of the Coulomb fluids [28]: the ion excess polarizability effects are relevant when electrostatic interactions are overall large and the dielectric discontinuities in the system are appreciable. Adding salt will normally lead to screening, and therefore diminishes the effects. However, it can also lead to *salt images*, an effect that has been discussed in Ref. [67].

An unresolved inconsistency of our methodology thus far is that the solvent is included on the implicit level and its polarizability is not taken explicitly into account. For an alternative treatment of these effects we refer to our recent work with a different electrostatic solver [27,38]. Nevertheless, our results lead to a better understanding of ionic polarization effects near charged interfaces and the methodology presented can be applied to other relevant cases, such as polarizable ionic liquids, the case we will consider in our future work.

JRB acknowledges the Brazilian science agencies CAPES for the financial support for a collaborative period at Institut für Computerphysik, Universität Stuttgart – scholarship No. 9155112 and CNPq for the financial suport under Grant No. 441712/2014-2. RP would like to acknowledge the financial support of the Agency for research and development of Slovenia under Grants No. N1-0019 and P1-0055 and the hospitality of the staff and the director of the ICP of the University of Stuttgart. CH acknowledges funding by the German Science Foundation (DFG) through the collaborative research centre SFB 716. We thank J. Zeman for a critical reading of the manuscript. In addition we wish K.K. a longlasting continuation of his fruitful scientific life and thank him for the many stimulating collaborations we had in the past.

References

1. J. Lyklema, *Fundamentals of Interface and Colloidal Science* (Academic London, 1995)
2. R.H. French, V.A. Parsegian, R. Podgornik, R.F. Rajter, A. Jagota, J. Luo, D. Asthagiri, M.K. Chaudhury, Y. Chiang, S. Granick, S. Kalinin, M. Kardar, R. Kjellander, D.C. Langreth, J. Lewis, S. Lustig, D. Wesolowski, J.S. Wettlaufer, W. Ching, M. Finnis, F. Houlihan, O.A. von Lilienfeld, C.J. van Oss, T. Zemb, Rev. Mod. Phys. **82**, 1887 (2010)
3. Y. Levin, Rep. Prog. Phys. **65**, 1577 (2002)
4. T. Markovich, D. Andelman, R. Podgornik, Charged Membranes: Poisson-Boltzmann theory, DLVO paradigm and beyond, Chapter 9 in: Handbook of Lipid Membranes, edited by C. Safynia, J. Raedler (Taylor & Francis, 2016)
5. A. Naji, M. Kanduč, R. Netz, R. Podgornik, *Understanding Soft Condensed Matter via Modeling and Computation*, Series in Soft Condensed Matter, Vol. 3, Chap. Exotic Electrostatics: Unusual Features of Electrostatics Interactions between Macroions (World Scientific, Singapore, 2010)
6. A.Y. Grosberg, T.T. Nguyen, B.I. Shklovskii, Rev. Mod. Phys. **74**, 329 (2002)
7. R. Messina, J. Phys.: Condens. Matter **21**, 113102 (2009)
8. A. Naji, M. Kanduč, J. Forsman, R. Podgornik, J. Chem. Phys. **139**, 150901 (2013)
9. D. Antypov, M.C. Barbosa, C. Holm, Phys. Rev. E **71**, 061106 (2005)
10. G.I. Guerrero-García, E. González-Tovar, M. Chávez-Paéz, M. Louzada-Cassou, J. Chem. Phys. **132**, 054903 (2010)
11. A.P. dos Santos, A. Diehl, Y. Levin, J. Chem. Phys. **130**, 124110 (2009)
12. M. Louzada-Cassou, R. Saavedra-Barrera, D. Henderson, J. Chem. Phys. **77**, 5150 (1982)
13. A. Naji, S. Jungblut, A.G. Moreira, R. Netz, Phys. A Stat. Mech. Appl. **352**, 131 (2005)
14. S. Pianegonda, M.C. Barbosa, Y. Levin, Europhys. Lett. **71**, 831 (2005)
15. A. Diehl, Y. Levin, J. Chem. Phys. **125**, 054902 (2006)
16. A. Diehl, Y. Levin, J. Chem. Phys. **129**, 124506 (2008)

17. G.I. Guerrero-García, E. González-Tovar, M.O. de la Cruz, Soft Matter **6**, 2056 (2010)
18. A.P. dos Santos, A. Diehl, Y. Levin, J. Chem. Phys. **132**, 104105 (2010)
19. T. Das, D. Bratko, L.B. Bhuiyan, C.W. Outhwaite, J. Phys. Chem. **99**, 410 (1995)
20. M.C. Barbosa, M. Deserno, C. Holm, Europhys. Lett. **52**, 80 (2000)
21. D. Ben-Yakoov, D. Andelman, R. Podgornik, J. Chem. Phys. **134**, 074705 (2011)
22. D. Ben-Yakoov, D. Andelman, R. Podgornik, D. Harries, Curr. Opin. Colloid Interface Sci. **16**, 542 (2011)
23. D. Frydel, J. Chem. Phys. **134**, 234704 (2011)
24. Y. Levin, A.P. dos Santos, A. Diehl, Phys. Rev. Lett. **103**, 257802 (2009)
25. Y. Levin, Phys. Rev. Lett. **102**, 147803 (2009)
26. V. Jadhao, F.J. Solis, M.O. de la Cruz, Phys. Rev. Lett. **109**, 223905 (2012)
27. F. Fahrenberger, O.A. Hickey, J. Smiatek, C. Holm, Phys. Rev. Lett. **115**, 118301 (2015)
28. V. Démeri, D.A. Dean, R. Podgornik, J. Chem. Phys. **137**, 174903 (2012)
29. P. Linse, J. Phys. Chem. **90**, 6821 (1986)
30. R. Messina, J. Chem. Phys. **117**, 11062 (2002)
31. K. Barros, E. Luijten, Phys. Rev. Lett. **113**, 017801 (2014)
32. A. Bakhshandeh, A.P. dos Santos, Y. Levin, Phys. Rev. Lett. **107**, 107801 (2011)
33. J.R. Bordin, A. Diehl, M.C. Barbosa, Y. Levin, Phys. Rev. E **85**, 031914 (2012)
34. Z. Xu, W. Cai, X. Cheng, Commun. Comput. Phys. **9**, 1056 (2010)
35. S. Tyagi, A. Arnold, C. Holm, J. Chem. Phys. **129**, 204102 (2008)
36. S. Tyagi, M. Suzen, M. Sega, M.C. Barbosa, S.S. Kantorovich, C. Holm, J. Chem. Phys. **132**, 145112 (2010)
37. F. Fahrenberger, Z. Xu, C. Holm, J. Chem. Phys. **141**, 064902 (2014)
38. F. Fahrenberger, C. Holm, Phys. Rev. E **90**, 063304 (2014)
39. F. Fahrenberger, O.A. Hickey, J. Smiatek, C. Holm, J. Chem. Phys. **143**, 243140 (2015)
40. Z. Wang, Y. Ma, J. Chem. Phys. **136**, 234701 (2012)
41. R. Messina, E.G. Tovar, M. Lozada-Cassou, C. Holm, Europhys. Lett. **60**, 383 (2002)
42. A. Martín-Molina, R. Hidalgo-Álvarez, M. Quesada-Pérez, J. Phys: Condens. Matter **21**, 424105 (2009)
43. G. Lamoureux, B. Roux, J. Chem. Phys. **119**, 3025 (2003)
44. G. Lamoureux, E. Harder, I.V. Vorobyov, B. Roux, A.D. MacKerell, Chem. Phys. Lett. **418**, 245 (2006)
45. V.M. Anisimov, G. Lamoureux, I.V. Vorobyov, N. Huang, B. Roux, A.D. MacKerrel Jr., J. Chem. Theory Comput. **1**, 153 (2005)
46. W. Yu, P.E.M. Lopes, B. Roux, A.D. MacKerell Jr., J. Chem. Phys. **138**, 034508 (2013)
47. J.A. Lemkul, J. Huang, B. Roux, A.D. MacKerell Jr., Chem. Rev. **116**, 4983 (2016)
48. B.T. Thole, Chem. Phys. **59**, 341 (1981)
49. G.L. Warren, S. Patel, J. Phys. Chem. C **112**, 7455 (2008)
50. H. Yu, T.W. Whitfield, E. Harder, G. Lamoureux, I.V. Vorobyov, V.M. Anisimov, A.D. MacKerrel Jr., B. Roux, J. Chem. Theory Comput. **6**, 774 (2010)
51. G. Archontis, E. Leontidis, G. Andreou, J. Phys. Chem. B **109**, 17957 (2005)
52. P.E.M. Lopes, J. Huang, J. Shim, Y. Luo, H. Li, B. Roux, A.D. MacKerell Jr., J. Chem. Theory Comput. **9**, 5430 (2013)
53. A. Savelyev, A.D. MacKerell Jr., J. Phys. Chem. B **118**, 6742 (2014)
54. C. Schröder, O. Steinhauser, J. Chem. Phys. **133**, 154511 (2011)
55. C. Schröder, Phys. Chem. Chem. Phys. **14**, 3089 (2012)
56. W.L. Jorgensen, J. Chem. Theory Comp. **3**, 1877 (2007)
57. H.J. Limbach, A. Arnold, B.A. Mann, C. Holm, Comput. Phys. Commun. **174**, 704 (2006)
58. A. Arnold, O. Lenz, S. Kesselheim, R. Weeber, F. Fahrenberger, D. Röhm, P. Košovan, C. Holm, in *Lecture Notes in Computational Science and Engineering*, **89**, edited by M. Griebel, M.A. Schweitzer (Springer Berlin Heidelberg, 2013), p. 1
59. A. Arnold, K. Breitsprecher, F. Fahrenberger, S. Kesselheim, O. Lenz, C. Holm, Entropy **15**, 4569 (2013)
60. M. Deserno, C. Holm, J. Chem. Phys. **109**, 7678 (1998)

61. P. Allen, D.J. Tildesley, *Computer Simulation of Liquids* (Oxford University Press, Oxford, 1987)
62. W. Jiang, D.J. Hardy, J.C. Phillips, A.D. MacKerrel Jr., K. Schulten, B. Roux, J. Phys. Chem. Lett. **2**, 87 (2011)
63. J.A. Lemkul, B. Roux, D. van der Spoel, A.D. MacKerell Jr., J. Comp. Chem. **36**, 1473 (2015)
64. C. Leung, H. Kinns, B.W. Hoogenboon, S. Howorka, P. Mesquisa, Nano Lett. **9**, 2769 (2009)
65. K. Umeda, K. Kobayashi, N. Oyabu, K. Matsishige, H. Yamada, Nanotech. **26**, 285103 (2015)
66. J.J. Molina, S. Lectez, S. Tazi, M. Salanne, J.-F. Dufrêche, J. Roques, E. Simoni, P.A. Madden, P. Turq, J. Chem. Phys. **134**, 014511 (2011)
67. M. Kanduč, A. Naji, J. Forsman, R. Podgornik, J. Chem. Phys. **137**, 174704 (2012)